PCCP

Accepted Manuscript

ROYAL SOCIETY OF CHEMISTRY

www.rsc.org/pccp

Physical Chemistry Chemical Physics

ARTICLE

Assignment of High-Lying Bending Mode Levels in the Threshold Photoelectron Spectrum of NH_2: A Comparison between Pyrolysis and Fluorine-Atom Abstraction Radical Sources

Received 00th January 20xx,
Accepted 00th January 20xx

DOI: 10.1039/x0xx00000x

www.rsc.org/

F. Holzmeier,[a] M. Lang,[a] I. Fischer,[a] P. Hemberger[b], G. A. Garcia,[c] X. Tang[c] and J.-C. Loison[d]

In this manuscript we present threshold photoelectron spectra (TPES) of the amidogen radical, NH_2, recorded at two vacuum ultraviolet synchrotron radiation beamlines, the DESIRS beamline of Synchrotron SOLEIL and the VUV beamline of the Swiss Light Source (SLS). Amidogen radicals were generated by two different methods, (a) H-atom abstraction of ammonia in a fluorine microwave discharge flow tube and (b) flash pyrolysis of methylhydrazine and diphenylmethylamine. Due to the large geometry change upon photoionization from the bent neutral molecule NH_2 ($\tilde{X}\ ^2B_1$) to the quasi-linear cation NH_2^+ ($\tilde{X}\ ^3B_1$), significant activity in the bending vibration υ_2^+ of NH_2^+ ($\tilde{X}\ ^3B_1$) is observed in the TPES. Transitions into a large number of υ_2^+, K_a^+ levels of the cation are resolved.

Introduction

Amidogen radical, NH_2 and its cation NH_2^+ have been detected in interstellar space[1-4] and appear in the combustion of ammonia[5] and in ammonia plasma processing[6]. From a molecular structure viewpoint the radical is also of interest because NH_2 is isoelectronic to H_2O^+ and NH_2^+ is isoelectronic to the carbene CH_2. Thus considerable effort has been made towards the spectroscopic characterization of both species.

The neutral amidogen in the $\tilde{X}\ ^2B_1$ electronic ground state has a bent structure with a HNH angle of around 102.4°,[7] while the $\tilde{X}\ ^3B_1$ ground state of the cation is quasi-linear with an energy minimum at 27.5° (bending angle) and a barrier to linearity of only 232 cm^{-1}.[8] The large geometry change upon photoionization leads to a significant activity in the bending mode υ_2^+, which provides detailed information on the potential energy surface of NH_2^+. However this also means that the Franck-Condon factors (FCF) at the ionization threshold are very small and one-photon ionization experiments challenging in this region. First data on the ionic structure of NH_2^+ were therefore obtained by infrared spectroscopy.[9] Photoion yield curves showed resonances that were assigned to Rydberg states converging to the first excited $\tilde{a}\ ^1A_1$ state.[10] A larger energy region was explored by conventional photoelectron spectroscopy,[11] but the lack of mass information, the presence of background signals (i.e. overlapping bands from ammonia) and the comparably low resolution rendered an assignment of individual vibrational states impossible. Merkt and coworkers investigated the cation by zero kinetic energy (ZEKE-) photoelectron spectroscopy in a [1+1′] process through the neutral $\tilde{A}\ ^2A_1$ state.[8] The ionization energies of the $\tilde{X}\ ^3B_1$ ground state[8] and the $\tilde{a}\ ^1A_1$ excited state were accurately determined to be 90 083.9 cm^{-1} and 100 306 cm^{-1} respectively.[8, 12] Furthermore, some low-lying vibrational levels were also observed and the barrier to linearity was determined.

Information on the higher-lying vibrational levels of NH_2 is on the other hand of relevance for the investigation of state-selected cations in ion-molecule reactions.[13] NH_2^+ is particularly interesting, because a large number of vibronic states are accessible by photoionization, so the reactivity can be in principle investigated over a large range of excess energies. Such experiments are motivated by the recent exploration of the atmosphere of Titan,[14] which showed the importance of nitrogen-containing species for the atmospheric chemistry.[15]

A suitable approach to study the ionic energy levels of reactive molecules is photoion-photoelectron coincidence (PEPICO) spectroscopy, in particular with tuneable VUV synchrotron sources where only threshold electrons can be selected and recorded, the so-called threshold PEPICO (TPEPICO) method. In this case, mass-selected threshold photoelectron spectra (TPES) with a comparably high resolution can be recorded. The technique is available at a few storage ring facilities[16, 17,18] because it exploits the easy tunability of these sources, and has been applied in recent years to a number of hydrocarbon radicals.[19] In the present manuscript we want to extend this work to the photoionization of NH_2. High-level computations on NH_2^+ are available for comparison.[20-23] Below we will in particular refer to the work by Chambaud et al, who computed vibronic energy levels on a three dimensional potential energy

[a] Institute of Physical and Theoretical Chemistry, University of Würzburg, Am Hubland, D-97074 Würzburg, Germany; E-mail: ingo.fischer@uni-wuerzburg.de
[b] Molecular Dynamics Group, Paul Scherrer Institut CH-5232 Villigen, Switzerland
[c] Synchrotron SOLEIL, L'Orme des Merisiers, St. Aubin, BP 48, 91192 Gif sur Yvette, France; E-mail: gustavo.garcia@synchrotron-soleil.fr
[d] ISM, Université Bordeaux 1, CNRS, 351 cours de la Libération, 33405 Talence Cedex, France; E-mail: jean-christophe.loison@u-bordeaux.fr

surface obtained from multireference configuration interaction (MRCI) electronic wavefunctions.[20]

One challenge in the study of reactive molecules is to efficiently generate radicals from a suitable precursor. Several approaches have been demonstrated, and three have been employed in conjunction with synchrotron radiation. The first is pyrolysis, i.e. thermal generation of the radical,[19, 24] which allowed the TPEPICO spectra of radicals like allyl,[25] methyl,[26] ethyl,[27] fulvenallenyl[28], phenylpropargyl[29, 30] and trifluoromethyl[31] to be recorded. The second method is through H-abstraction reaction by fluorine atoms produced in a microwave discharge, which has recently been applied to record the photoionization spectra of OH,[32] OD[32], ethyl[27] and H_2CN radicals.[33] A similar source has been employed before by Dyke and coworkers to record conventional photoelectron spectra of radicals,[34, 35] among them NH_2.[11] The third one is photodissociation of a suitable precursor, as in the cases of methylene,[36] methyl,[37] vinyl,[38] propargyl,[38] allyl,[39] propenyl[39] or phenyl radical[40]. Two of these approaches, pyrolysis and H-abstraction by fluorine atoms, have been employed here to continuously generate the amidogen radical and measure TPEPICO spectra. In this manuscript we compare the two approaches and describe the two complementary studies. One study was conducted at the Swiss Light Source (SLS) storage ring and generates amidogen by pyrolysis, while the other one, carried out at Synchrotron SOLEIL, employs the fluorine atom source.

Experimental

At the third generation French synchrotron SOLEIL, the vacuum ultraviolet (VUV) photons delivered by the HU640 variable polarization undulator feeding the DESIRS beamline [41] were monochromatised and focused onto a 200/100 μm (H/V) spot at the ionization region. A 200 grooves·mm^{-1} SiC grating was chosen and the slits were set to obtain a photon energy resolution of 3 meV at 11.5 eV for a flux of $7x10^{11}$ photons/sec. The gas filter[42] located upstream the monochromator was filled with 0.24 *mbar* of Ar, effectively cutting off higher order radiation from the undulator. The energy dependent data were normalized by the photon flux recorded via a dedicated photodiode (AXUV, IRD) and the energy scale was calibrated during the same scan by the absorption lines seen in the total ion yield due to the 4s and 4s' absorption lines[43] from the Ar in the gas filter, leading to an energy precision of $\pm$ 0.0015 eV. After photoionization, electrons and ions were detected in coincidence using a double imaging photoelectron/photoion coincidence spectrometer (i^2PEPICO) described elsewhere[17]. The coincidence scheme allows tagging the photoelectron spectra (PES) in mass and in ion translational energy. The latter is used here to discriminate electrons and ions correlated to targets that are formed outside the reactor.[32] Threshold electrons are obtained with a resolution of 10 meV *via* the slow PES technique or SPES[44], which leads to resolutions comparable to the more common threshold PES [45] (TPES), but with a higher signal-to-noise ratio.

At the VUV beamline of the Swiss Light Source a bending magnet provides synchrotron radiation which was collimated and diffracted by a plane grating (600 grooves·mm^{-1}) with a resolving power of around 10^4 and a flux on the order of some 10^{11} photons/*sec*. A rare gas filter operated with a Kr/Ar/Ne mixture at a pressure of 10 mbar suppresses the higher harmonic radiation. The experimental setup is equipped with a time-of-flight mass spectrometer and a velocity map imaging photoelectron spectrometer. Ions and electrons were collected in coincidence, yielding mass-selected threshold photoelectron spectra (ms-TPES). The beamline and spectrometer are described in more detail elsewhere.[46, 47] The photon energy was scanned in steps of 5 meV and threshold electrons were selected with an energy resolution of 5 meV. The contribution of background electrons was subtracted following the method of Sztaray and Baer.[45]

In the SLS experiment NH_2 radicals were generated by flash pyrolysis from two different precursors, methyl hydrazine, H_2N-NH(CH_3) and diphenylmethylamine (DPMA), $(C_6H_5)_2$-CH-NH_2, both commercially obtained from Sigma-Aldrich, expanded in Ar through a 100 µm orifice into an electrically heated SiC tube. DPMA had to be heated to 175 °C to generate a sufficient vapour pressure. The setup used at SOLEIL has been described recently.[32] For this study, NH_2 radicals were generated through the F + NH_3 -> HF + NH_2 reaction in a fast flow tube at low pressure (typically 1 to 2 mbar of mainly He). Fluorine atoms were produced in a microwave discharge of a mixture of 1% F_2 diluted in He (Linde), introduced into the flow tube 50 cm before the reaction zone. NH_3 was introduced into the reactor through the showerhead mixer at the tip of the injector. The F_2 concentration was around 3×10^{13} molecules cm^{-3}. The F_2 dissociation efficiency is close to 80% (checked trough F_2 detection after photoionisation) and considering the wall losses, the initial NH_2 concentration range is estimated at around 4×10^{13} molecules cm^{-3}. After passage through the flow tube, the mixture is adiabatically expanded through a first skimmer (ϕ=1 *mm* diameter home-made in Kel-F) into a differentially pumped chamber (few 10^{-4} mbar), and through a second skimmer (ϕ=1 *mm*, Beam Dynamics Inc.) into the ionization chamber (few 10^{-8} *mbar*).

Results and discussion

Molecular composition of the flow-tube reactor.

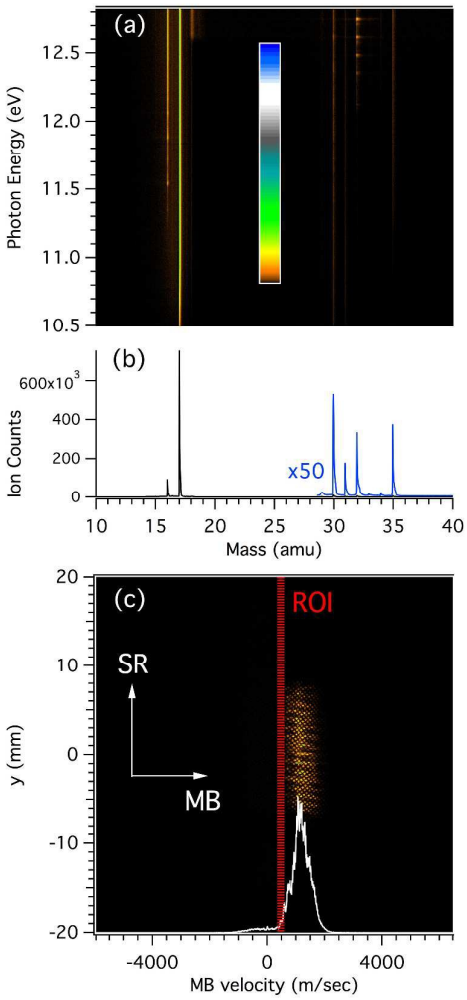

Figure 1: (a) Ion signal as a function of m/z and photon energy. (b) TOF integrated between 12.5 and 12.8 eV. (c) Mass-selected ion image and its projection (white line) along the molecular beam (MB) axis. Only ions having a net velocity (>500 m/sec) along MB fall within the region of interest (ROI) and are taken into account, corresponding to the species present in the flow-tube, and avoiding the background gas.

Mass spectra (MS) as a function of the photon energy are shown as a color matrix in Figure 1a. As mentioned in the previous section, species formed outside the flow-tube reactor will be discriminated because only data correlated with ions inside the region of interest (ROI) shown in Figure 1c will be added to the treatment. A single MS integrated between 12.5 and 12.8 eV photon energy is also presented in Figure 1b. The main species in the molecular beam are *m/z* 16 (NH_2) and *m/z* 17 (NH_3), with traces of *m/z* 15 (NH), *m/z* 18 (H_2O), *m/z* 30 (NO), *m/z* 31 (HNO), *m/z* 32 (O_2) and *m/z* 35 (NH_2F). The F + NH_3 reaction shows a high rate constant at room temperature[48] characteristic of a barrierless reaction, producing only NH_2 + HF, the $NH_3 + F \rightarrow NH_2F + H$ reaction is calculated here to be endothermic by 150 kJ/mol at the M06-2X/cc-pVTZ level (using Gaussian 09)[49]. The presence of traces of NH and NH_2F is likely due to the secondary $NH_2 + F \rightarrow NH + HF / NH_2F$ reaction. Note that the chemical structures corresponding to the mass peaks have been verified by their mass-selected PES and comparison to existing literature. Indeed, both spectrometers at SOLEIL and SLS record simultaneously the electron spectra of all the masses present, so that the same information shown in this article for *m/z* 16 is available for the rest. In Figure 1a, autoionization resonances can be clearly observed for O_2, as bright spots over the continuum background. They are also visible for NH_2. From the NH_2 ion image shown in Figure 1c, a velocity of 1180 m/sec is extracted, its value and spread consistent with a translational temperature of the order of 170 K.

Molecular composition of the pyrolysis reactor

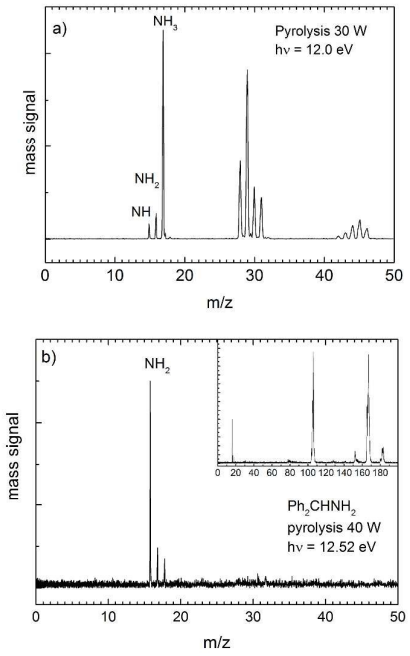

Figure 2: TOF mass spectra of the pyrolytic NH_2 precursors: a) In methylhydrazine (*m/z*=46) pyrolysis ammonia, NH_3 constitutes the most intense peak, but several other masses are visible as well. b) When diphenylmethylamine is employed, the amount of ammonia can be significantly reduced, but larger aromatic molecules are present.

The idea in pyrolysis is to select a suitable precursor and thermally cleave the weakest bond. In the case of amidogen different precursors are available, as visible in the mass spectra in Figure 2. Trace a) shows the generation of amidogen from methyl hydrazine, H_2N-$NH(CH_3)$, m/z=46, recorded at the fixed photon energy hν = 12.0 eV. A small amount of residual precursor is still present while ammonia is the most intense peak in the mass spectrum, indicating a more complicated chemistry than originally thought, but a small peak at *m/z*=16, corresponding to NH_2 is also apparent. In addition there is a second group of peaks present at *m/z*=28-31. The peaks at *m/z*=28 and 29 correspond to the cations of H_2CN and H_2CNH. The TPES of both species have been presented in a recent publication[50] that also discusses the mass spectrum in more detail. Masses 31 and 30 are due to methylamine, H_3C-NH_2 and its dissociative ionization fragment ion H_2C-NH_2. A second precursor is DPMA (*m/z*=183),

Figure 2b). Pyrolysis forms predominately the benzhydryl radical (*m/z*=167) plus NH_2, while diphenylmethylcarbene (*m/z*=166) plus NH_3 is a minor channel.[51] Due to lower vapour pressure of the precursor, signals are smaller, but the NH_2/NH_3 ratio is more favorable.

Threshold Photoelectron Spectra

Amidogen is an asymmetric rotor. In the ground state of the cation, rotational constants of A^+=155.08 cm^{-1}, B^+= 8.38 cm^{-1} and C^+=7.95 cm^{-1} were computed in the MRCI calculations.[20] The resulting asymmetry parameter is κ=-0.99, so NH_2^+ can be regarded as an almost linear prolate rotor with well separated *K*-stacks. For the bending vibration of NH_2^+ a wavenumber of 850 cm^{-1} was reported from a He (I) photoelectron spectrum,[11] but the mode is strongly anharmonic due to the shape of the potential energy surface. Therefore we expect to resolve well separated, but irregularly spaced levels in the spectra that are characterized by a vibrational quantum number υ_2^+ and an angular momentum quantum number K_a^+.

In a quasilinear molecule either bent molecule quantum numbers υ_2^+, K_a^+, N^+ can be used for the bending vibration, or linear molecule quantum numbers $\upsilon_2^{+|K|}(lin), N^+$. The two quantum numbers are related via the expressions.

$$\upsilon_2^+ (lin) = 2\upsilon_2^+ (bent) + K_a^+ \quad \text{(I)}$$

$$|K| = K_a^+ \quad \text{(II)}$$

The total rotational angular momentum N^+ will be largely ignored below, because it can hardly be resolved. As the spectral assignments below are based on the calculations by Chambaud et al,[20] who used the bent-molecule nomenclature, we will also assign transitions using the bent molecule labels υ_2^+, K_a^+, N^+ . Note however that Merkt and coworkers employed the linear molecule labelling scheme in their work.[8]

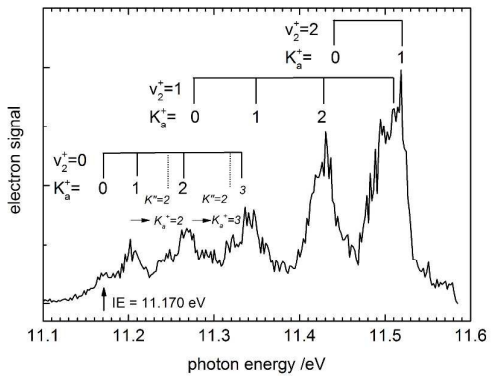

Figure 3: TPES of NH_2, recorded at the SOLEIL storage ring with a 2 meV photon energy step. Unless otherwise indicated the transitions originate from K_a" =0 and 1.

Figure 3 shows the TPES of NH_2 around the ionization threshold, recorded at SOLEIL with a 2 meV photon energy step. Although the transition into the υ_2^+ =0, K_a^+ =0 ground state of the cation is weak, it can definitely be recognized, and transitions into the K_a^+ =1-3 states are clearly discernible despite the unfavorable FC-factors. The values agree fully with those reported by Willitsch et al.[8] Note that for example the υ_2^+ =0, K_a^+ =1 level corresponds to 1^1 in the linear molecule notation. The peaks at 11.25 eV and 11.32 eV might be assigned to transitions from the thermally populated K_a"=2 level in the neutral ground state. Note that the K_a"=1 and 2 levels are 24.7 cm^{-1} and 94.4 cm^{-1} above the K_a"=0 level. The $\Delta N=N^+-N$" transitions cannot be resolved for the most part and broaden the various *K*-stacks. Some bands, for example the one between 11.50 and 11.55 eV show evidence of ΔN structure. Since several $\Delta K=K_a^+-K_a$" transitions contribute to this band, it is rather difficult to fit the rotational fine structure, because transitions from K_a" =1 cannot be distinguished from those originating from K_a"=0.

TPES were recorded using both setups at SOLEIL and SLS up to the onset of the $\tilde{a}\ ^1A_1$ state, as depicted in Figure 4. The band positions are summarized in Table 1 and compared to previous work. Like the $\tilde{X}\ ^2B_1$ neutral ground state, the $\tilde{a}\ ^1A_1$ ionic state is also bent, thus diagonal FC-factors are large and the transition into the υ_2^+ =0 origin band is the most intense in the spectrum. A value of 12.436 eV (100 306 cm^{-1}) was reported by Willitsch et al.[12] The maximum of the TPES recorded at SOLEIL is located at 12.428±0.002 eV. After adding the 7 meV Stark shift corresponding to the 88 V/cm^{-1} extraction field used in these experiments, a value of 12.435±0.002 eV is reached, in perfect agreement with the aforementioned ZEKE experiments

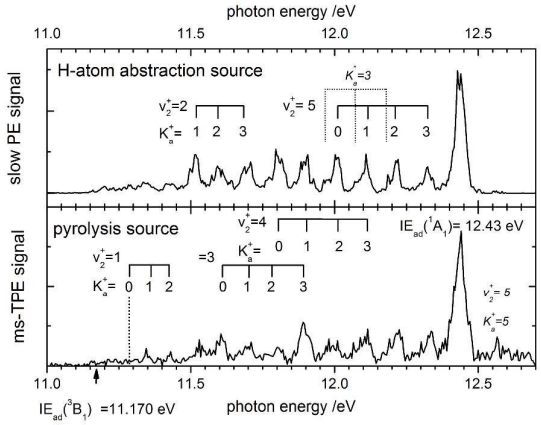

Figure 4: Survey scan of NH_2^+. The spectrum in the upper trace was recorded at SOLEIL, using the H- atom abstraction radical source, the one in the lower trace was recorded at the SLS using pyrolysis of DPMA to generate NH_2.

Both spectra in Figure 4 have a similar appearance. Transitions into the K_a^+ stacks of υ_2^+ =5 can be resolved and the intensities of the various transitions are comparable in both spectra. The maximum intensity is found for the members of υ_2^+ =4. Transitions into υ_2^+ =6 are not unambiguously identified and thus already considerably weaker. In both spectra transitions into K_a^+=0-3 can be recognized. In the previous ZEKE experiments only transitions into ionic states up to υ_2^+ =2, K_a^+ =0 were reported,[8] corresponding to 4^0 in linear notation. Several peaks show a shoulder to the left shifted by 25-30 meV, especially visible in the members of the υ_2^+ =4 and 5 series. Some of them are indicated by dotted lines in the upper trace of Figure 4. They might be due to transitions from K_a"=3 at +27 meV. In the SLS spectrum these shoulders are indistinguishable from the

main peak, indicating a larger population of the K_a"=3 levels. This leads to a somewhat inferior resolution of the spectrum and indicates a higher internal temperature of the radicals. The present results agree well with the computations by Chambaud *et al.*[20] and almost all spectral features can be unambiguously assigned. The error between the present results and the computed values is generally within 10 meV. Although Chambaud *et al*. did not compute transitions into higher K_a" states, most features can be assigned without taking them into account. Given the spectral resolution one can analyse the photoionization selection rules for ΔK transitions. The framework for rotational transitions in photoionization has been developed in detail by Merkt and coworkers.[52, 53] In a simplified picture for NH_2 an electron is ejected upon ionization from a non-bonding *p*-orbital located at the nitrogen atom. From the orbital ionization model[52] one would expect in this case the selection rule $\Delta K_a = \pm 1$. Of course the population in higher K_a" levels has to be considered. At the experimental temperatures the K_a"=1 level will be almost equally populated as the K_a"=0 one. Since it is only 24 cm^{-1} higher in energy, transitions originating from the K_a"=0 and K_a"=1 levels cannot be resolved. Transitions from K_a"=2 are also present, which also explains the pronounced appearance of K_a^+ =3 even within the orbital ionization model. However, there are indications that the simple $\Delta K_a = \pm 1$ selection rule is not fully obeyed. In Figure 3 the transitions from K_a"=2 to υ_2^+ =0, K_a^+ =2 and from K_a"=0, 1 to υ_2^+ =0, K_a^+ =3 can be recognized. For the first one, which is only weakly present, no other credible assignment is found. The transition into υ_2^+ =0, K_a^+ =3 on the other hand overlaps with the one into υ_2^+ =1, K_a^+ =1. Assigning the whole band around 11.34 eV to the latter transition would lead to an energy that is too low when compared with the value known accurately from ZEKE-spectroscopy (see column 3 of Table 1). We are therefore convinced that transitions with $\Delta K_a = 0, \pm 2$ contribute to the spectrum and reflect deviations from a simple single orbital picture. Overall the intensity seems to decrease with increasing K_a^+, which probably reflects the thermal population in the neutral ground state. Transitions into K_a^+ =3 were not observed in the ZEKE-spectra recorded in a pulsed jet of 30 K rotational temperature.

At the experimental temperatures ground state levels with K_a"=3 are likely populated and some transitions are tentatively assigned to originate from K_a"=3. Thus transitions into K_a^+ =4 should also be visible. However, they are difficult to assign, because accurate calculations are not available for K_a">3. Nevertheless the pyrolysis spectrum shows a band at 12.56 eV (+1.39 eV) that might be assigned to υ_2^+ =5, K_a^+ =5 (note its absence in the H-abstraction source), while the υ_2^+ =5, K_a^+ =4 band most likely overlaps with the strong transition into the $\tilde{A}\ ^2A_1$ origin. Overall transitions into K_a^+ =4 will already have a considerably smaller intensity and often contribute to a broadening of bands only.

The TPES obtained from pyrolysis of methylhydrazine (not shown here) and DPMA have a rather similar appearance. However, when methylhydrazine is employed, the NH_2 signal rises again at 12.6 eV. This rise is due to dissociative photoionization of either unconverted precursor or, more likely, a side product of the pyrolysis.

Transitions into the stretching modes υ_1^+ and υ_3^+ are not observed in the spectra. Due to the small change in the R(N-H) bond length upon ionization from 1.034 Å to 1.030 Å the FC-factors into the fundamentals and overtones of these modes are small.[20, 54]

Table 1: List of the observed transitions, with previous experimental and computational results given for comparison. Unless otherwise indicated the transitions originate from K_a" =0 and 1.

Transition υ_2^+, K_a^+	This work /eV	Prev. experiment, Ref [8]	Computations /eV, Ref. [20]
0, 1	0.038	0.0396	0.040
K"=2→ 0, 2	0.078		
0, 2	0.096	0.0938	0.094
1, 0	0.106	0.1138	0.113
K"=2→ 0, 3	0.151		
0, 3	0.166		0.159
1, 1	0.176	0.1830	0.183
1, 2	0.26	0.2567	0.257
2, 0	0.268	0.2672	0.266
1, 3	0.339		0.337
2, 1	0.35		0.351
2, 2	0.43		0.438
3, 0	0.43		0.443
2, 3	0.52		0.529
3, 1	0.54		0.538
3, 2	0.63		0.633
4, 0	0.63		0.636
3, 3	0.72		0.734
4, 1	0.74		0.742
4, 2	0.84		0.843
5, 0	0.84		0.845
4, 3	0.94		0.947
5, 1	0.94		0.951
K"=3→5, 2	1.02		
5, 2	1.05		1.058
5, 3	1.15		
5, 5	1.39		

Comparison of Radical Sources

As the experiments were performed at different beamlines a comparison is not straightforward. We note that the photon flux at the DESIRS beamline was probably higher by a factor of 2 or more, so a larger signal can be expected.

The H-atom abstraction source yields the precursor ammonia, NH_3, as the most intense peak in the mass spectrum. In contrast in the pyrolysis source the ratio amidogen/ammonia depends on the precursor: Pyrolysis of methylhydrazine yields a NH_2/NH_3 ratio that is almost the same as in the H-atom abstraction source and seems to be around 0.15. The large amount of ammonia is surprising, because its formation requires bimolecular reactions. When DPMA is employed as a precursor the NH_2/NH_3 ratio is around 5:1 and

favours amidogen formation. This will be an advantage, when experiments are perturbed by NH_3, but the overall signal is smaller due to the low vapour pressure of DPMA. Nevertheless it is evident from the mass spectra in Figures 1b and 2 that the H-abstraction source is cleaner than the pyrolysis source. This may be due to the fact that all the H-atoms in ammonia have the same reaction probability.

The most important difference between the two spectra in Figure 4 is the resolution, which is higher with the H-abstraction source. A possible reason for this is the different temperatures of the radicals. Regarding the production by H abstraction, the available energy from the $F + NH_3 \rightarrow HF + NH_2$ reaction is equal to ΔH=-117 kJ/mol.[55] The energy partitioning of this reaction has also been experimentally studied.[56] A large part of the energy is localized in the HF vibration in a similar manner than for the $F + CH_4 \rightarrow HF + CH_3$ reaction[57] where very little energy is reallocated in the CH_3 vibrations or rotations. Moreover, the self-reaction $NH_2 + NH_2$ is slow at low pressure and leads only to N_2H_4[58] so that we can use conditions where the NH_2 radicals stay a few ms in the fast flow reactor at 1 *Torr*, allowing efficient rotational and vibrational relaxation. At 1.0 *Torr* of He in the presence of few *mTorr* of NH_3, we can assume that all internal degrees of freedom of the NH_2 radical have been thermalized before expansion through the 1.0 *mm* diameter homemade Kel-F skimmer. With a backing pressure of only a few *mbar*, the translational temperature of the NH_2 after adiabatic expansion has been determined at 170 *K* (see Figure 1b), and we expect the rotational and vibrational temperatures of NH_2 to be between this value and 294 *K* (room temperature).

When combined with pulsed jets, cold radicals have been obtained in pyrolysis sources due to a supersonic expansion into the vacuum. For several radicals rotational temperatures of around 100-150 *K* have been determined.[59, 60] However, the situation changes in continuous beams: While in pulsed beams nozzle orifices of around 0.8 *mm* are combined with the pyrolysis reactor (ID=1.0 *mm*), in continuous beams orifices of 0.1-0.2 *mm* are often employed to limit the gas load. The subsequent reduction of the particle density by more than an order of magnitude changes the properties of the flow and reduces the number of radical/rare gas collisions in the pyrolysis reactor and at the exit. As a consequence a supersonic jet does not fully develop and only limited cooling is achieved.[61] For example the TPES of methyl[26] was fitted with a rotational temperature of 500 *K,* while a temperature of 350 *K* was estimated in the case of $CF_3^{\bullet}$.[31] The higher temperature is evident in the observation of some transitions into K_a^+ >3. Furthermore the longer residence time of the molecules in the pyrolysis reactor and the high concentration of the precursor leads to a larger degree of bimolecular reactions. This has already been observed in some of the first experiments combining pyrolysis and SR[62] and is also evident in the mass spectrum of methylhydrazine pyrolysis (5-10% methylamine in argon), cf. Figure 2a). The most intense peak is NH_3, which has to be formed by an H-atom abstraction reaction of amidogen.

Conclusions

Amidogen radical, NH_2 has been produced by two different methods: H-atom abstraction in a fluorine discharge flow tube, using ammonia as the precursor, and flash pyrolysis of methylhydrazine and of diphenylmethylamine, at the storage rings Synchrotron SOLEIL and SLS repectively. The bending level structure of the quasilinear $\tilde{X}\ ^3B_1$ ground state of NH_2^+ has been studied by threshold photoelectron spectroscopy. The radical was ionized in a one-photon process from the bent $\tilde{X}\ ^2B_1$ neutral ground state using VUV synchrotron radiation. The bending level progression of NH_2^+ ($\tilde{X}\ ^3B_1$) has been observed and assigned up to $\upsilon_2^+ \leq 5$ and $K_a^+ \leq 3$, here labels refer to the bent-molecule notation. Despite the large geometry change even transitions close to the ionization threshold were observed. While the spectra are very similar, the radicals generated in the fluorine discharge have a rotational temperature T_{rot}=170-294 *K*, while for the radicals generated by pyrolysis T_{rot}=500 *K* is likely. As a consequence the spectra obtained by H-atom abstraction are better resolved. In the pyroylsis source on the other hand the NH_2/NH_3 ratio can be varied using different precursors, which can be an advantage for example for studying dissociative photoionisation. In addition to the ionic ground state the $\tilde{a}\ ^1A_1$ state has been observed. This bent - bent transition is dominated by the origin band observed at 12.435±0.002 eV.

The results presented will be of value for studies of ion-molecule reactions involving NH_2^+ due to the large impact that the amount of internal energy can have on the outcome of the reaction.[63] In this context NH_2^+ is an excellent candidate for studying the reactivity of a molecular ion over a wide range of vibrational and rotational excitation.

Acknowledgements

The pyrolysis experiments were carried out a the VUV X04DB beamline of the Swiss Light Source, Paul Scherrer Institut (PSI), Villigen, Switzerland This work has been financially supported by the German Science Foundation through contract FI 575/7-x and the Swiss Federal Office for Energy (BFE Contract Number 101969/152433). The flow-tube experiments have received financial support from the French Agence Nationale de la Recherche (ANR) under grant ANR-12-BS08-0020-02 (project SYNCHROKIN). JC, XT and GAG are indebted to J.-F. Gil and L. Nahon for their technical and scientific help as well as to the general SOLEIL staff for running the facility under proposal n° 20130929. The contribution of Michael Ward and Sébastien Batut to the acquisition of the flow-tube data is warmly acknowledged. IF acknowledges stimulating discussions with the members of the graduate research school GRK 2112.

Notes and references

1 E. van Dishoeck, D. J. Jansen, P. Schilke and T. G. Phillips, *ApJ*, 1993, **416**, L83.

2 P. Hily-Blant, S. Maret, A. Bacmann, S. Bottinelli, B. Parise, E. Caux, A. Faure, E. A. Bergin, G. A. Blake, A. Castets, C. Ceccarelli, J. Cernicharo, A. Coutens, N. Crimier, K. Demyk, C. Dominik, M. Gerin, P. Hennebelle, T. Henning, C. Kahane, A. Klotz, G. Melnick, L. Pagani, P. Schilke, C. Vastel, V. Wakelam, A. Walters, A. Baudry, T. Bell, M. Benedettini, A. Boogert, S.

Cabrit, P. Caselli, C. Codella, C. Comito, P. Encrenaz, E. Falgarone, A. Fuente, P. F. Goldsmith, F. Helmich, E. Herbst, T. Jacq, M. Kama, W. Langer, B. Lefloch, D. Lis, S. Lord, A. Lorenzani, D. Neufeld, B. Nisini, S. Pacheco, T. Phillips, M. Salez, P. Saraceno, K. Schuster, X. Tielens, F. van der Tak, M. H. D. van der Wiel, S. Viti, F. Wyrowski and H. Yorke, *A&A*, 2010, **521**, L52.

3 C. M. Persson, J. H. Black, J. Cernicharo, J. R. Goicoechea, G. E. Hassel, E. Herbst, M. Gerin, M. De Luca, T. A. Bell, A. Coutens, E. Falgarone, P. F. Goldsmith, H. Gupta, M. Kazmierczak, D. C. Lis, B. Mookerjea, D. A. Neufeld, J. Pearson, T. G. Phillips, P. Sonnentrucker, J. Stutzki, C. Vastel, S. Yu, F. Boulanger, E. Dartois, P. Encrenaz, T. R. Geballe, T. Giesen, B. Godard, C. Gry, P. Hennebelle, P. Hily-Blant, C. Joblin, R. Kolos, J. Krelowski, J. Martin-Pintado, K. Menten, R. Monje, M. Perault, R. Plume, M. Salez, S. Schlemmer, M. Schmidt, D. Teyssier, I. Péron, P. Cais, P. Gaufre, A. Cros, L. Ravera, P. Morris, S. Lord and P. Planesas, *A&A*, 2010, **521**, L45.

4 C. M. Persson, M. De Luca, B. Mookerjea, A. O. H. Olofsson, J. H. Black, M. Gerin, E. Herbst, T. A. Bell, A. Coutens, B. Godard, J. R. Goicoechea, G. E. Hassel, P. Hily-Blant, K. M. Menten, H. S. P. Müller, J. C. Pearson and S. Yu, *A&A*, 2012, **543**, A145.

5 C. Duynslaeger, F. Contino, J. Vandooren and H. Jeanmart, *Combust. Flame*, 2012, **159**, 2799.

6 C. I. Butoi, M. L. Steen, J. R. D. Peers and E. R. Fisher, *J. Phys. Chem. B*, 2001, **105**, 5957.

7 C. Jungen, K.-E. Hallin and A.-J. Merer, *Mol. Phys.*, 1980, **40**, 25.

8 S. Willitsch, C. Jungen and F. Merkt, *J. Chem. Phys.*, 2006, **124**, 204312.

9 Y. Kabbadj, T. R. Huet, D. Uy and T. Oka, *J. Mol. Spectrosc.*, 1996, **175**, 277.

10 S. T. Gibson, J. P. Greene and J. Berkowitz, *J. Chem. Phys.*, 1985, **83**, 4319.

11 S. J. Dunlavey, J. M. Dyke, N. Jonathan and A. Morris, *Mol. Phys.*, 1980, **39**, 1121.

12 S. Willitsch, J. M. Dyke and F. Merkt, *Mol. Phys.*, 2004, **102**, 1543.

13 N. Carrasco, C. Alcaraz, O. Dutuit, S. Plessis, R. Thissen, V. Vuitton, R. Yelle and P. Pernot, *Planet. Space Sci.*, 2008, **56**, 1644.

14 T. Owen, *Nature*, 2005, **438**, 756.

15 V. Vuitton, R. V. Yelle and V. G. Anicich, *ApJ*, 2006, **647**, L175.

16 A. Bodi, M. Johnson, T. Gerber, Z. Gengeliczki, B. Sztáray and B. T., *Rev. Sci. Instrum.*, 2009, **80**, 034101.

17 G. A. Garcia, B. K. Cunha de Miranda, M. Tia, S. Daly and L. Nahon, *Rev. Sci. Instrum.*, 2013, **84**, 053112.

18 X. Tang, X. Zhou, M. Niu, S. Liu, J. Sun, X. Shan, F. Liu and L. Sheng, *Rev. Sci. Instrum.*, 2009, **80**, 113101.

19 C. Alcaraz, D. Schröder and I. Fischer, in *Encyclopedia of Radicals in Chemistry, Biology and Materials*, eds. C. Chatgilialoglu und A. Studer, John Wiley & Sons, Chichester, 2012, vol. 1, pp. 477.

20 G. Chambaud, W. Gabriel, T. Schmelz, P. Rosmus, A. Spielfiedel and N. Feautrier, *Theor. Chim. Acta*, 1993, **87**, 5.

21 P. Jensen, P. R. Bunker and A. D. McLean, *Chem. Phys. Lett.*, 1987, **141**, 53.

22 V. J. Barclay, I. P. Hamilton and P. Jensen, *J. Chem. Phys.*, 1993, **99**, 9709.

23 G. Osmann, P. R. Bunker, P. Jensen and W. P. Kraemer, *J. Mol. Spectrosc.*, 1997, **186**, 319.

24 D. W. Kohn, H. Clauberg and P. Chen, *Rev. Sci. Instrum.*, 1992, **63**, 4003.

25 T. Schüßler, H.-J. Deyerl, S. Dümmler, I. Fischer, C. Alcaraz and M. Elhanine, *J. Chem. Phys.*, 2003, **118**, 9077.

26 B. K. Cunha de Miranda, C. Alcaraz, M. Elhanine, B. Noller, P. Hemberger, I. Fischer, G. Garcia, H. Soldi-Lose, B. Gans, L. A. Viera Mendez, S. Boye-Peronne, S. Douin, J. Zabka and P. Botschwina, *J. Phys. Chem. A*, 2010, **114**, 4818.

27 B. Gans, G. A. Garcia, S. Boye-Peronne, J.-C. Loison, S. Douin, F. Gaie-Levrel and D. Gauyacq, *J. Phys. Chem. A*, 2011, **115**, 5387.

28 M. Steinbauer, P. Hemberger, I. Fischer and A. Bodi, *ChemPhysChem*, 2011, **12**, 1795.

29 P. Hemberger, M. Steinbauer, M. Schneider, I. Fischer, M. Johnson, A. Bodi and T. Gerber, *J. Phys. Chem. A*, 2009, **114**, 4698.

30 F. Holzmeier, M. Lang, P. Hemberger and I. Fischer, *ChemPhysChem*, 2014, 3489.

31 H. Dossmann Soldi-Lose, G. A. Garcia, L. Nahon, B. K. Cunha de Miranda and Alcaraz, *J. Chem. Phys.*, 2012, **136**, 204304.

32 G. A. Garcia, X. Tang, J.-F. Gil, L. Nahon, M. Ward, S. Batut, C. Fittschen, C. A. Taatjes, D. L. Osborn and J.-C. Loison, *J. Chem. Phys.*, 2015, **142**, 164201.

33 F. L. Nesbitt, G. Marston, L. J. Stief, M. A. Wickramaaratchi, W. Tao and R. B. Klemm, *J. Phys. Chem.*, 1991, **95**, 7613.

34 J. Baker, M. Barnes, M. C. R. Cockett, J. M. Dyke, A. M. Ellis, M. Feher, E. P. F. Lee, A. Morris and H. Zamanpour, *J. Electron Spectrosc.*, 1990, **51**, 487.

35 J. D. Barr, L. Beeching, A. De Fanis, J. M. Dyke, S. D. Gamblin, N. Hooper, A. Morris, S. Stranges, J. B. West, A. E. Wright and T. G. Wright, *J. Electron Spectrosc. Relat. Phenom.*, 2000, **108**, 47.

36 M. Litorja and B. Ruscic, *J. Chem. Phys.*, 1998, **108**, 6748.

37 C. A. Taatjes, D. L. Osborn, T. M. Selby, G. Meloni, H. Fan and S. T. Pratt, *J. Phys. Chem. A*, 2008, **112**, 9336.

38 J. C. Robinson, N. E. Sveum and D. M. Neumark, *J. Chem. Phys.*, 2003, **119**, 5311.

39 J. C. Robinson, N. E. Sveum and D. M. Neumark, *Chem. Phys. Lett.*, 2004, **383**, 601.

40 N. E. Sveum, S. J. Goncher and D. M. Neumark, *Phys. Chem. Chem. Phys.*, 2006, **8**, 592.

41 L. Nahon, N. de Oliveira, G. A. Garcia, J. F. Gil, B. Pilette, O. Marcouille, B. Lagarde and F. Polack, *J. Synchrotron Radiat.*, 2012, **19**, 508.

42 B. Mercier, M. Compin, C. Prevost, G. Bellec, R. Thissen, O. Dutuit and L. Nahon, *J. Vac. Sci. Tech. A*, 2000, **18**, 2533.

43 W. F. Chan, G. Cooper, X. Guo, G. R. Burton and C. E. Brio, *Phys. Rev. A*, 1992, **46**, 149.

44 J. C. Poully, J. P. Schermann, N. Nieuwjaer, F. Lecomte, G. Grégoire, C. Desfrançois, G. A. Garcia , L. Nahon, D. Nandi, L. Poisson and M. Hochlaf, *Phys. Chem. Chem. Phys.*, 2010, **12**, 3566.

45 B. Sztáray and T. Baer, *Rev. Sci. Instrum.*, 2003, **74**, 3763.

46 M. Johnson, A. Bodi, L. Schulz and T. Gerber, *Nucl. Instrum. Meth. A*, 2009, **610**, 597.

47 A. Bodi, P. Hemberger, T. Gerber and B. Sztaray, *Rev. Sci. Instrum.*, 2012, **83**, 083105.

48 A. Persky, *Chem. Phys. Lett.*, 2007, **439**, 3.

49 R. A. Gaussian 09, Frisch, M. J.; Trucks, G. W.; Schlegel, H. B.; Scuseria, G. E.; Robb, M. A.; Cheeseman, J. R.; Scalmani, G.; Barone, V.; Mennucci, B.; Petersson, G. A.; Nakatsuji, H.; Caricato, M.; Li, X.; Hratchian, H. P.; Izmaylov, A. F.; Bloino, J.; Zheng, G.; Sonnenberg, J. L.; Hada, M.; Ehara, M.; Toyota, K.; Fukuda, R.; Hasegawa, J.; Ishida, M.; Nakajima, T.; Honda, Y.; Kitao, O.; Nakai, H.; Vreven, T.; Montgomery, Jr., J. A.; Peralta, J. E.; Ogliaro, F.; Bearpark, M.; Heyd, J. J.; Brothers, E.; Kudin, K. N.; Staroverov, V. N.; Kobayashi, R.; Normand, J.; Raghavachari, K.; Rendell, A.; Burant, J. C.; Iyengar, S. S.; Tomasi, J.; Cossi, M.; Rega, N.; Millam, N. J.; Klene, M.; Knox, J. E.; Cross, J. B.; Bakken, V.; Adamo, C.; Jaramillo, J.; Gomperts, R.; Stratmann, R. E.; Yazyev, O.; Austin, A. J.; Cammi, R.; Pomelli, C.; Ochterski, J. W.; Martin, R. L.; Morokuma, K.; Zakrzewski, V. G.; Voth, G. A.; Salvador, P.; Dannenberg, J. J.; Dapprich, S.; Daniels, A. D.; Farkas, Ö.; Foresman, J. B.; Ortiz, J. V.; Cioslowski, J.; Fox, D. J. , *Gaussian, Inc., Wallingford CT, 2009*.

50 F. Holzmeier, M. Lang, K. Hader, P. Hemberger and I. Fischer, *J. Chem. Phys.*, 2013, **138**, 214310.

51 M. Lang, F. Holzmeier, I. Fischer and P. Hemberger, *J. Phys. Chem. A*, 2013, **117**, 5260.

52 S. Willitsch and F. Merkt, *Int. J. Mass Spectrom.*, 2005, **245**, 14.

53 R. Signorell and F. Merkt, *Mol. Phys.*, 1997, **92**, 793.

54 J. W. C. Johns, D. A. Ramsay and S. C. Ross, *Can. J. Phys.*, 1976, **54**, 1804.

55 D. L. Baulch, C. T. Bowman, C. J. Cobos, R. A. Cox, T. Just, J. A. Kerr, M. J. Pilling, D. Stocker, J. Troe, W. Tsang, R. W. Walker and J. Warnatz, *J. Phys. Chem. Ref. Data*, 2005, **34**, 757.

56 A. S. Manocha, D. W. Setser and M. A. Wickramaaratchi, *Chem. Phys.*, 1983, **76**, 129.

57 J. Zhou, J. J. Lin, W. Shiu, S.-C. Pu and K. Liu, *J. Chem. Phys.*, 2003, **119**, 2538.

58 K. Fagerstrom, J. T. Jodkowski, A. Lund and E. Ratajczak, *Chemical Physics Letters*, 1995, **236**, 103.

59 I. Fischer and P. Chen, *J. Phys. Chem. A*, 2002, **106**, 4291.

60 J. Giegerich, I. Fischer, J. Petersen and R. Mitric, *Phys. Chem. Chem. Phys.*, 2014, **16**, 6294.

61 Q. Guana, K. N. Urnessa, T. K. Ormond, D. E. David, G. B. Ellison and J. W. Daily, *Int. Rev. Phys. Chem.*, 2014, **33**, 447.

62 I. Fischer, T. Schüßler, H.-J. Deyerl, M. Elhanine and C. Alcaraz, *Int. J. Mass Spectrom.*, 2007, **261**, 227.

63 B. K. Cunha de Miranda, C. Romanzin, S. Chefdeville, V. Vuitton, J. Zabka, M. Polasek and C. Alcaraz, *J. Phys. Chem. A*, 2015, **119**, 6082.

TOC Figure

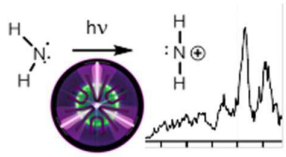

The bending mode progression in the photoelectron spectrum of NH_2 was observed and assigned up to $\upsilon_2^+ \leq 5$ and $K_a^+ \leq 3$.